SAND--98-8451C
CONF-980804--

Hydrogen Flame Suppression by CF_3I

Andrew McIlroy
Sandia National Laboratories
Livermore, CA

Brian Brady
The Aerospace Corporation
El Segundo, CA

Paul Marshall
University of North Texas
Denton, TX

Word Count:

Section	Count	Method
Text and Table:	4141	Word
Figures:	1400	7×200
Total:	5541	

Corresponding Author:
Andrew McIlroy
Sandia National Laboratories
MS 9055
Livermore, CA 94551-0969
USA
Phone (510) 294-3054
Fax (510) 294-2276
Email: amcilr@ca.sandia.gov

DISCLAIMER

Introduction

Halons have long been the fire suppressants of choice for applications requiring high performance. The bromine containing halons possess a unique set of properties: very low extinguishing concentrations (<5% by volume), clean application with no residue, low toxicity, and they are electrically and chemically inert. The halons found use in a wide variety of applications: computer rooms, oil refineries and storage facilities, military and civilian aircraft. The halons derive their unique fire suppression properties primarily from catalytic action of the bromine atoms they contain. Bromine has been shown to participate in several catalytic chemical cycles that lead to the recombination of important combustion chain carriers, such as hydrogen atoms, to form stable species. However, halons are linked to the stratospheric ozone depletion problem. The most common halon, 1301 or CF_3Br, has an ozone depletion potential (ODP) 11 times higher than the most common chlorofluorocarbon (CFC) refrigerant. This has led to a ban on halon production under the Clean Air Act legislation in the United States following the Montreal Protocols on ozone depleting substances.[1]

Halon replacements are being actively sought for new fire suppression systems and to retrofit existing systems as the current supply of halons is exhausted. One promising replacement is CF_3I. This compound has been shown to have fire suppression performance similar to that achieved for halon 1301, but with a very low ODP.[2] Unlike halon 1301, CF_3I rapidly photolyzes in the troposphere, and thus has a tropospheric lifetime of less than two days.[3] However, CF_3I is not the perfect replacement; it has performed poorly in cardiac sensitization studies and is approved only for total flooding applications in unoccupied spaces and streaming

applications.[2] As for any chemical fire suppressant, it is useful to understand the chemical mechanisms which lead to suppression in order to optimize performance, and minimize the formation of potentially hazardous combustion byproducts such as HF, HI, and CF_2O.

In this study, we seek to build a model for the suppression of hydrogen fires by CF_3I. Hydrogen fires are of both practical and scientific interest. Hydrogen is used as a high performance rocket fuel, appears in substantial quantities in the petroleum refining process and has the potential for being a zero emission fuel. However, hydrogen is also a significant fire and explosion hazard. The minimum ignition energies for hydrogen are more than a factor of ten lower than for common hydrocarbon fuels, and hydrogen is flammable in air from 5% to 95% by volume.[4] Thus the development of a high performance, environmentally acceptable hydrogen fire suppressant is desirable. From a fundamental viewpoint, the hydrogen combustion mechanism is appealing because it is the simplest and best characterized of all combustion mechanisms, and an important sub-mechanism of all hydrocarbon combustion mechanisms. Thus, a high-performance hydrogen fire suppressant would almost certainly be an excellent suppressant for most other common fires.

Several previous studies have investigated the detailed combustion kinetics of CF_3X (X=Br,I) either by experimental or theoretical means. Biordi and coworkers carried out the first comprehensive flame studies of $CH_4/O_2/Ar/CF_3Br$ combustion using a laminar, premixed, low-pressure flame and a molecular beam sampling mass spectrometer.[5-8] Recently, Johnson and McIlroy investigated the flame structure of a laminar, premixed, low pressure $CH_4/O_2/Ar/CF_3I$

flame using a probe sampling mass spectrometer.[9] Battin-Leclerc and coworkers have used a perfectly stirred reactor to investigate the slow oxidation of the $CH_4/O_2/Ar/CF_3X$ (X=Br,I) systems.[10,11] Westbrook developed the first comprehensive flame model for hydrogen and methane flames inhibited by CF_3Br.[12.13] More recently, Babushok and coworkers have introduced an improved mechanism for CF_3X (X=Br,I) fire suppression.[14,15] Little of this work has concentrated on the suppression of hydrogen flames.

In this contribution, we present a new mechanism for the suppression of hydrogen combustion by CF_3I. This model is compared to new experimental results from low-pressure $H_2/O_2/Ar/CF_3I$ flame studies. One-dimensional, laminar flame calculations are used to determine the major fire suppression mechanisms of CF_3I. The remainder of the paper is organized as follows: First the model is described in detail. Second, the experimental method and results are presented. Finally, we compare the model and experimental results and discuss the major reaction pathways and suppression mechanisms of CF_3I in hydrogen flames.

Model Description

The detailed chemical kinetic reaction mechanism for the suppression of hydrogen fires by CF_3I was constructed from a combination of literature reaction mechanisms and new rate data. The hydrogen oxidation mechanism is that of Miller and coworkers.[16] Since CF_3I is likely to be present in only low concentrations, some assumptions are made to simplify the reaction set. First, we assume that except for reaction including CF_3I itself, we can neglect reactions of iodine

and fluorine containing species. The rates of these reactions should be slow, and the low concentration of the species relative to fuel and oxidizer species should make these reactions negligible in a flame. Next, we assume that the low concentration of CF_n species makes the formation of C_2F_m or larger species slow compared to other processes. Thus only C1 chemistry is included in the reaction mechanism. Finally, we neglect the CH_nF_m species since their formation reactions should be slow in hydrogen flames because the only sources of hydrogen are H, H_2, OH, HO_2 and H_2O. Except for HO_2, none of these species have readily extractable hydrogens and recombination of CF_n species with H atoms should be slow. Previous studies of flame suppression by hydrofluorocarbons have shown these to be reasonable assumptions. To describe the decomposition of CF_3, we use the reaction set of McIlroy and Johnson.[9]

Several recent experimental and theoretical studies have improved our understanding of the elementary reactions of iodine compounds. Kumaran et al. have characterized the unimolecular decomposition of CF_3I in a shock tube.[17] Bimolecular reactions of CF_3I with the major flame radicals H, OH and O have been studied by the pulsed photolysis - resonance fluorescence technique.[18] The radicals were generated by flash lamp and/or excimer laser photolysis of precursors (NH_3 for H atoms, H_2O for OH and O_2 and SO_2 for O) on a microsecond or shorter time scale, in the presence of a large excess of CF_3I. The radicals then reacted under pseudo-first-order conditions over millisecond time scales. Because the radical concentration was kept very small, below about 10^{12} molecule cm^{-3}, self-reaction and consumption by photolysis or reaction products was minimized, so that the desired elementary reactions were isolated from competing processes. The radical concentration was monitored as a function of time with

microsecond resolution by means of UV or vacuum UV resonance fluorescence excited by a microwave-powered lamp. The fluorescence signals were detected via photon counting and signal averaging. The results for the reactions

$$CF_3I + H \rightarrow CF_3 + HI$$

$$CF_3I + OH \rightarrow CF_3 + HOI$$

$$CF_3I + O \rightarrow CF_3 + IO$$

are summarized in Table I. Computational studies of the potential energy surface indicate that the third reaction proceeds via a bound CF_3IO intermediate, which under combustion conditions will dissociate to $CF_3 + IO$.

Some of the H-O-I rate constants are available from the literature [19, 20], but many needed to be estimated. Gaussian-2 (G2) theory, as extended to iodine-containing species [21], was applied to characterize reactants, products and transition states (TSs) for individual reactions. Briefly, molecular geometries and vibrational frequencies were obtained at the MP2/6-31G(d) level of theory [22] and were employed to compute the partition functions Q for each species. Single-point energies were computed at the G2 level of theory, which approximates a complete QCISD(T)/6-311+G(3d,2p) calculation, and used to derive reaction enthalpies and energy barriers $E_0^{\ddagger}$. The ab initio data were employed in canonical transition state theory (TST): [23]

$$k_{TST} = \Gamma \frac{k_B T}{h} \frac{Q_{TS}}{Q_{Reactants}} \exp\left(-\frac{E_o^{\ddagger}}{RT}\right)$$

Γ is a correction term for quantum mechanical tunneling, and hindered internal rotors are also treated in this analysis. Rate constants for the following processes were obtained [24]:

$$O + HI \rightarrow OH + I$$

$$I + H_2O_2 \rightarrow HI + HO_2$$

$$IO + H_2 \rightarrow HOI + H$$

The rate constant for O + HI → OH + I is already known experimentally [19], and we found excellent accord between theory and experiment for this reaction. TST was employed to extrapolate the measurements to combustion temperatures. No reaction barrier was found for

$$OH + HI \rightarrow H_2O + I$$

in accord with recent measurements [25]. A number of other rate constants were guessed. H + I recombination was assumed to be equal to H + Br recombination [19] while the exothermic processes 64-66 in Table I were assumed to have negligible barriers and thus rate constants close to gas kinetic. Reactions 59-61 are likely to proceed via bound intermediates with small barriers to formation and dissociation, so we have assumed these reactions have high rate constants also. For the unimolecular dissociation of HOI, the activation energy was set equal to a recently estimated I-O bond strength [18], together with a guessed pre-exponential factor.

Table I lists the complete reaction set and rate parameters. Laminar flame species and temperature profiles were calculated using the Sandia PREMIX code which utilizes the CHEMKIN chemistry and TRANLIB transport subroutines.[26-29] All calculations were performed in the burner-stabilized mode with a calculated temperature profile.

Experimental Methods and Results

The low-pressure flame apparatus utilized in this study has been described fully elsewhere[9], and only a brief description is included here. A McKenna flat flame burner is housed in a 6-way cross, 8" diameter, copper seal cross. Gas is supplied to the burner through mass flowcontrollers calibrated to a standard volumetric flowmeter. A servo controlled throttle valve in the exhaust line maintains the flame chamber pressure. The burner is translated vertically and all diagnostics are space-fixed. The primary diagnostic is a microprobe sampling mass spectrometer. Since the previous description of this apparatus, a new probe has been designed which minimizes flame attachment. The probe is constructed from a ¼" diameter quartz tube drawn to a fine tip. The orifice diameter of the probe is approximately 100 μm and the wall thickness at the tip is approximately 30 μm. With this probe, there is no visible flame attachment in stoichiometric methane flames at 30 torr, and stable species profiles in both methane and hydrogen flames agree well with predicted profiles without shifting the experimental profiles. The probe to mass spectrometer distance has also been shortened to ~40 cm.

The data presented here were collected at a flame chamber pressure of 30.0 torr and a total mass flow rate of approximately 0.0018 g cm^{-3} s^{-1}. The hydrogen flame had a mixture ratio of $H_2/O_2/Ar$=0.22/0.11/0.67. The mole fraction of CF_3I was varied over the range 0.000-0.030 while the hydrogen flame stoichiometry was maintained constant. The symbols in Fig. 1a show the concentration profiles of the stable species as a function of burner height for the undoped

flame, and Fig. 1b shows the concentration profiles for a flame with 0.006 mole fraction CF_3I added to the flame. The relative extent of inhibition as a function of CF_3I concentration can be measured from the height of the flame above the burner surface. Here we define the flame front position as the half-height of the water profile. Figure 2 displays experimental (symbols) and calculated (lines) flame front positions as a function of suppressant concentration.

Discussion

Comparison of Model and Experimental Data

One qualitative measure of the suppression effect of CF_3I is the rise of flame front off the burner surface with increasing suppressant concentration. Figure 2 shows a plot of flame front height versus mole fraction of CF_3I for both the experimental and calculated flames. At 30 torr, the stoichiometric hydrogen flame lifts slightly off the burner with the addition of CF_3I, but then stays at a constant height off the burner until just before the flame blows out at a mole fraction of 0.03. The calculation predicts a similar behavior, although a slight dip near 0.02 is predicted, but not observed. The calculated flames rise rapidly from the burner at concentrations above 0.03, in good agreement with concentration at which the experimental flames becoming unstable. The calculated rise from the burner coincides with a calculated drop in the flame speed and an increase in the flame temperature. Although the reduction in flame speed is expected for an inhibitor, the rise in the flame temperature is not an obvious sign of suppression. The temperature rise is the result of the exothermic formation of HF, one of the primary products of the CF_3 group oxidation.

The measured stable species concentration profiles show good agreement with the calculated values, as shown in Fig. 1b. Of particular interest is the rapid destruction of CF_3I early in the flame zone. The experimental profile for [CF_3I] falls off slower than the calculated profile, but still shows the suppressant to be destroyed in the preheat zone of the flame. The weak C-I bond is largely responsible for the early disappearance of CF_3I.

Reaction Path and Suppression Mechanisms

The detailed model results give insight into the probable fire suppression mechanisms of CF_3I. First, we examine the predicted concentration profiles as a function of height above burner. Previous authors have shown that CF_3Br acts to catalyze hydrogen atom recombination through a bromine-based cycle. We can find evidence for this by comparing the H-atom concentration profiles for CF_3I doped and undoped flames. Figure 3 shows that less H-atom and more hydrogen molecules are present in the doped flame. The differences are most pronounced at temperatures below 1000 K.

The fluorine based chemistry in the flame functions mainly to produce HF from CF_3I. Although this serves as a radical trap, it is of limited efficiency since one F-atom traps only one H-atom. The CF_3 radicals are destroyed in an oxidative path that goes primarily through CF_2O and CFO to produce CO and CO_2. Our limited fluorine reaction set reproduces this path well and is in good agreement with hydrofluorocarbon oxidation calculations based on a much more complete

fluorine reaction set.[14,15] The fluorine chemistry then does not explain the rise in hydrogen molecules and loss of H-atoms early in the flame.

This leads us to consider the iodine chemistry, and its role in H-atom recombination. Figure 4 shows the calculated concentration profiles of the iodine species. These profiles show that at temperatures above 1000 K, iodine exists primarily as I-atom due to the weak nature of iodine bonds. The primary iodine carrier in the region between the destruction of CF_3I and the transition to I-atom is HI, an important part of most hydrogen atom recombination cycles. Throughout the flame, the oxygenated iodine species are found to exist at only low concentrations. Molecular iodine is present only in trace quantities due to the weak I-I bond.

Figures 5 and 6 show the rates of iodine reactions in the first 1.0 cm of the 30 torr flame. As expected from the concentration profiles, all of the reactions take place in the first 0.40 cm of the flame at temperatures below 800 K. The three reactions proceeding at the fastest rates are shown in Fig. 5. The model predicts the primary loss mechanism for CF_3I to be iodine abstraction by H atom. In the hydrogen flame, thermal decomposition of CF_3I is predicted to be unimportant, and indeed recombination of CF3 and I is one of the fastest reactions. The recombination

$$CF_3 + I \rightarrow CF_3I$$

is driven by production of I and CF_3 from

$$H + CF_3I \rightarrow HI + CF_3 \text{ and}$$

$$H + HI \rightarrow H_2 + I.$$

These two reactions combined with the recombination reaction produce a fast catalytic cycle for the conversion of H-atoms to molecular hydrogen. This cycle is analogous to the methyl based H-atom recombination cycle identified in a $CF_3I/CH_4/O_2$ jet-stirred reactor by Battin-Leclerc and coworkers.[11] Here the CF_3 group takes the place of methyl. Although the CF_3 cycle was likely present in the jet-stirred reactor work, the large concentration of methyl radicals would have rendered it relatively unimportant.

Figure 6 shows the remaining iodine reactions with net rates above 10^{-8} mole cm^{-3} s^{-1}. Note that these reactions are all 50-100 times slower than the fast reactions in Fig. 5. We find that the H-atom recombination cycle

$$H + HI \rightarrow H_2 + I$$

$$H + I_2 \rightarrow HI + I$$

$$I + I \rightarrow I_2,$$

analogous to that identified by Westbrook for bromine atoms[13], is active, although the second two reactions are proceeding slowly compared to the first. A third cycle is also active

$$H + HI \rightarrow H_2 + I$$

$$H + I \rightarrow HI.$$

A more complex cycle which forms water from H-atoms and O-atoms takes place, but is slow, and no rise in early water production is observed.

$$O + HI \rightarrow OH + I$$

$$OH + HI \rightarrow H_2O + I$$

$$I + I \rightarrow I_2$$

$$H + I_2 \rightarrow HI + I$$

$$H + I \rightarrow HI$$

Figure 7 summarizes the iodine reaction pathways in the early portion of the flame near 0.20 cm. Not surprisingly for a hydrogen flame, H-atom reactions are most important. Overall, the oxygenated iodine reactions are found to be of minor importance to hydrogen fire suppression by CF_3I.

Conclusion

A new reaction mechanism for suppression of hydrogen fires by CF_3I has been developed. Good agreement has been found between model and experiment results over the limited experimental range of species and conditions probed. However, more detailed data is needed to test the model definitively. Four hydrogen radical recombination catalytic cycles are identified which contribute to hydrogen fire suppression. One of the cycles is new and makes use of the CF_3 radical in a manner analogous to the CH_3 radical suppression cycle observed previously. The CF_3 based cycle is responsible for most of the H-atom recombination in this flame.

Acknowledgments

AM thanks the U.S. Department of Energy, Office of Basic Energy Sciences, Chemical Sciences Division for support. BB was supported by the U. S. Air Force under contract F04701-93-C-0094. PM thanks the AFOSR, U.S. Air Force Wright Laboratory, R. A. Welch Foundation and UNT Faculty Research Fund for support.

References

[1] Anderson, S. O., Metchkis, K. L. and Rubenstein, R., *Halon Replacements: Technology and Science* (A. W. Miziolek and W. Tsang, Eds.), American Chemical Society, Washington, DC, 1995, p. 175.

[2] Tapscott, R. E., Skaggs, S. R. and Dierdorf, D., *Halon Replacements: Technology and Science* (A. W. Miziolek and W. Tsang, Eds.), American Chemical Society, Washington, DC, 1995, p. 151.

[3] Solomon, S., Burkholder, J. B., Ravishankara, A. R. and Garcia, R. R., *J. Geophys. Res.* 99:20929-20935 (1994).

[4] Glassman, I., Combustion (3rd ed) Academic Press, San Diego, 1996, pp. 581-607.

[5] Biordi, J. C., Lazzara, C. P. and Papp J. F., "Using Molecular Beam Mass Spectrometry. Reaction Rates and Mechanism in a 0.3% CF_3Br Inhibited Flame," U. S. Bur. Mines Rept. of Investigations RI8029, 1975.

[6] Biordi, J. C., Lazzara, C. P. and Papp, J. F., *Fifteenth Symposium (International) on Combustion,* The Combustion Institute, Pittsburgh, PA, 1975, pp. 917-.

[7] Biordi, J. C., Lazzara, C. P. and Papp, J. F., *J. Phys. Chem.* 81:1139 (1977).

[8] Biordi, J. C., Lazzara, C. P. and Papp, J. F., *J. Phys. Chem.* 82:125 (1978).

[9] McIlroy, A. and Johnson, L. K., *Combust. Sci. and Tech.* 116-117:31-50 (1996).

[10] Battin-Leclerc, F., Come, G. M., and Baronnet, F., *Combustion and Flame* 99:644-652(1994).

[11] Battin-Leclerc, Glaude, P. A., F., Come, G. M., and Baronnet, F., *Combustion and Flame* 109:285-292 (1997).

[12] Westbrook, C. K., *Nineteenth Symposium (International) on Combustion,* The Combustion Institute, Pittsburgh, PA, 1982, pp.127-141.

[13] Westbrook, C. K., *Combust. Sci. and Tech.* 34:201-225(1983).

[14] Babushok V., Noto T., Burgess D. R. F., Hamins A. and Tsang W., *Combustion and Flame* 107:351-367 (1996).

[15] Babushok V., Noto T., Burgess D. R. F., Hamins A. and Tsang W., *Combustion and Flame* 108:61-70 (1997).

[16] Thorne, L. R., Branch, M. C., Chandler, D. W., Kee, R. J., and Miller, J. A., *Twenty-First Symposium (International) on Combustion,* The Combustion Institute, Pittsburgh, 1986, p. 965-.

[17] Kumaran, S.S., Su., M-C., Lim, K. P., Michael, J. V., *Chem. Phys. Lett.* 243:59-63 (1995).

[18] Yuan, J. Misra, A., Wells, L., Hawkins, S., Krishnan, A., Nathuji, R. B., Marshall, P., Berry, R. J., Fourth *International Conference on Chemical Kinetics,* paper J5 (1997).

[19] Baulch, D. L., Duxbury, J., Grant, S. J., Montague, D. C., *Evaluated Kinetic Data for High Temperature Reactions Vol. 4, J. Phys. Chem. Ref. Data* 10:supplement no. 1 (1981).

[20] Atkinson, R., Baulch, D. L., Cox, R. A., Hampson, R. F.,Jr., Kerr, J. A., Troe, J. *Evaluated kinetic and photochemical data for atmospheric chemistry. Supplement IV, J. Phys. Chem. Ref. Data_*21:1125-1568 (1992).

[21] Glukhovtsev, M. N., Pross, A., McGrath, M. P. and Radom, L. *J. Chem. Phys.*, **103**, 1878-1885 (1995).

[22] Frisch M. J., Trucks, G. W., Schlegel, H. B., W. Gill, P. M., Johnson, B. G., Robb, M. A., Cheeseman, J. R., Keith, T., Petersson, G. A., Montgomery, J. A., Raghavachari, K., Al-Laham, M. A., Zakrzewski, V. G., Ortiz, J. V., Foresman, J. B., Peng, C. Y., Ayala, P. Y., Chen, W., Wong, M. W., Andres, J. L., Replogle, E. S., Gomperts, R., Martin, R. L., Fox, D. J., Binkley, J. S., Defrees, D. J., Baker, J., Stewart, J. J. P., Head-Gordon, M., Gonzalez, C., and Pople, J. A., *GAUSSIAN 94* (Gaussian, Pittsburgh, PA, 1995).

[23] Steckler, R., Hu, W.-P., Liu, Y.-P.,. Lynch, G. C, Garrett, B. C., Isaacson, A. D., Lu, D.-H., Melissas, V. S., Truong, T. N., Rai, S. N., Hancock, G. C., Lauderdale, J. G., Joseph, T. and Truhlar, D. G., POLYRATE - version 6.5 (University of Minnesota, Minneapolis, 1995).

[24] Misra, A., Berry, R. J., Marshall, P. *unpublished work.*

[25] Campuzano-Jest, P., Crowley, J. N., Moortgat, G. K., *Fourteenth International Symposium on Gas Kinetics*, paper C10 (1996).

[26] Kee, R. J., Dixon-Lewis, G., Warnatz, J., Coltrin, M. E., and Miller, J. A., "A Fortran Computer Code Package for the Evaluation of Gas-Phase Multicomponent Transport Properties," Sandia National Laboratories Report No. SAND86-8246.UC-32, 1986.

[27] Kee, R. J., Grcar, J. F., Smooke, M. D., and. Miller, J. A., "A Fortran Program for Modeling Steady Laminar One-Dimensional Flames," Sandia National Laboratories Report No. SAND85-8240.UC-4, 1987.

[28] Kee, R. J., Rupley, F. M., and Miller, J. A. , "Chemkin II: A Fortran Chemical Kinetics Package for the Analysis of Gas-Phase Chemical Kinetics," Sandia National Laboratories Report No. SAND89-8009.UC-401, 1991.

[29] Kee, R. J., Rupley, F. M., and Miller, J. A., "The Chemkin Thermodynamic Database," Sandia National Laboratories Report No. SAND87-8251B.UC-4, 1991.

[30] Amphlett, J.C., Whittle, E. Trans. Faraday Soc. **63**: 2695-2701 (1967).

Table I: Chemical kinetic reaction mechanism for $H_2/O_2/CF_3I$ combustion. $k=AT^b\exp(-E/RT)$

	Reaction	A [mole-cm-sec-K]	B	E (cal/mole)	Ref.
1.	$H_2+O_2=2OH$	1.70E+13	0.0	47780.0	16
2.	$H_2+OH=H_2O+H$	1.17E+09	1.3	3626.0	16
3.	$H+O_2=OH+O$	5.13E+16	-.8	16507.0	16
4.	$O+H_2=OH+H$	1.80E+10	1.0	8826.0	16
5.	$H+O_2+M=HO_2+M$	2.10E+18	-1.0	0.0	16
6.	$H+O_2+O_2=HO_2+O_2$	6.70E+19	-1.4	0.0	16
7.	$OH+HO_2=H_2O+O_2$	5.00E+13	0.0	1000.0	16
8.	$H+HO_2=2OH$	2.50E+14	0.0	1900.0	16
9.	$O+HO_2=O_2+OH$	4.80E+13	0.0	1000.0	16
10.	$2OH=O+H_2O$	6.00E+08	1.3	0.0	16
11.	$H+H+M=H_2+M$	1.00E+18	-1.0	0.0	16
12.	$H+H+H_2=2H_2$	9.20E+16	-.6	0.0	16
13.	$H+H+H_2O=H_2+H_2O$	6.00E+19	-1.3	0.0	16
14.	$2O+M=O_2+M$	1.41E+17	-1.0	398.0	16
15.	$H+OH+M=H_2O+M$	7.50E+23	-2.6	0.0	16
16.	$H+HO_2=H_2+O_2$	2.50E+13	0.0	700.0	16
17.	$HO_2+HO_2=H_2O_2+O_2$	2.00E+12	0.0	0.0	16
18.	$H_2O_2+M=2OH+M$	1.30E+17	0.0	45500.0	16
19.	$H_2O_2+H=HO_2+H_2$	1.60E+12	0.0	3800.0	16
20.	$H_2O_2+OH=H_2O+HO_2$	1.00E+13	0.0	1800.0	16
21.	$H+HF=H_2+F$	2.19E+14	0.0	33740.0	9
22.	$H+F_2=HF+F$	1.20E+14	0.0	2400.0	9
23.	$F+F+M=F_2+M$	1.00E+14	0.0	0.0	9
24.	$H+F+M=HF+M$	9.55E+17	-1.0	0.0	9
25.	$CF_3+H=HF+CF_2$	3.98E+12	0.0	0.0	9
26.	$CF_3+O=CF_2:O+F$	1.29E+14	0.0	2000.0	9
27.	$CF_3+OH=CF_2:O+HF$	3.98E+12	0.0	0.0	9
28.	$CF_3+O_2=CF_3O+O$	2.26E+09	1.1	21500.0	9
29.	$CF_3O+M=CF_2:O+F$	9.03E+26	-3.4	21700.0	9
30.	$CF_3O+H=CF_2:O+HF$	1.00E+14	0.0	0.0	9
31.	$CF_3O+H_2=>CF_3OH+H$	1.00E+13	0.0	5000.0	9
32.	$CF_3O+H_2O=>CF_3OH+OH$	0.00E+00	0.0	5000.0	9
33.	$CF_3OH=>CF_2:O+HF$	1.00E+14	0.0	43000.0	9
34.	$CF_2:O+H=CF:O+HF$	1.29E+11	0.0	0.0	9
35.	$CF_2+H=HF+CF$	1.00E+13	0.0	0.0	9
36.	$CF_2+O=CF:O+F$	1.00E+13	0.0	0.0	9
37.	$CF_2+OH=CF:O+HF$	1.00E+13	0.0	0.0	9
38.	$CF_2+OH=CF_2:O+H$	1.00E+13	0.0	0.0	9
39.	$CF:O+M=F+CO+M$	1.44E+14	0.0	30000.0	9
40.	$CF:O+H=HF+CO$	2.00E+14	0.0	0.0	9
41.	$CF:O+O=CO+FO$	1.00E+14	0.0	0.0	9
42.	$CF:O+OH=CO+HFO$	1.00E+14	0.0	0.0	9
43.	$CF:O+OH=CO_2+HF$	1.00E+14	0.0	0.0	9
44.	$CF_3I+M=CF_3+I+M$	1.95E+15	0.0	34350.0	17
45.	$CF_3I+H=CF_3+HI$	4.09E+13	0.0	950.0	18
46.	$CF_3I+O=CF_3+IO$	1.02E+13	0.0	620.0	18
47.	$CF_3I+OH=CF_3+HOI$	1.75E+08	1.5	1910.0	18
48.	$CF_3I+I=CF_3+I_2$	7.40E+13	0.0	17800.0	31
49.	$I_2+M=I+I+M$	8.25E+13	0.0	30300.0	19
50.	$H+I_2=HI+I$	4.31E+14	0.0	430.0	19
51.	$O+I_2=IO+I$	8.43E+13	0.0	0.0	20
52.	$OH+I_2=HOI+I$	1.08E+14	0.0	0.0	20
53.	$H+HI=H_2+I$	4.74E+13	0.0	660.0	19
54.	$O+HI=OH+I$	1.51E+07	2.0	0.0	24
55.	$OH+HI=H_2O+I$	3.61E+13	0.0	0.0	25
56.	$H+I+M=HI+M$	1.92E+21	-1.9	0.0	a
57.	$I+HO_2=HI+O_2$	9.03E+12	0.0	2170.0	20
58.	$I+H_2O_2=HI+HO_2$	2.29E-03	4.7	17630.0	24
59.	$IO+O=I+O_2$	1.81E+13	0.0	0.0	a
60.	$IO+H=OH+I$	1.81E+13	0.0	0.0	a
61.	$IO+OH=HO_2+I$	1.81E+13	0.0	0.0	a
62.	$IO+H_2=HOI+H$	2.09E-09	6.4	5650.0	24
63.	$IO+HO_2=HOI+O_2$	3.85E+13	0.0	0.0	20
64.	$HOI+O=IO+OH$	1.50E+13	0.0	0.0	a
65.	$HOI+OH=IO+H_2O$	6.00E+12	0.0	0.0	a
66.	$IO+H_2O_2=HOI+HO_2$	6.00E+12	0.0	0.0	a
67.	$HOI+M=OH+I+M$	6.00E+13	0.0	50000.0	a

a. This work.

Figure Captions

Figure 1: a) Comparison of calculated and experimental data for stable species in an undoped, stoichiometric hydrogen/oxygen flame at P=30 torr. Experimental data is taken with a probe sampling mass spectrometer. b) Comparison of calculated and experimental data for stable species with the addition of 0.006 mole fraction CF_3I.

Figure 2: Experimental and calculated flame front height above burner (solid line) and calculated peak temperature (dashed line) as a function of CF_3I mole fraction in a stoichiometric hydrogen/oxygen flame at P=30.0 torr. The concentration at which the experimental flame could no longer be stabilized on the burner is noted.

Figure 3: Calculated mole fractions of hydrogen atom and hydrogen molecule in flames with and without CF_3I as a function of height above burner. Also shown are the ratios of the doped and undoped mole fractions for H and H_2 to demonstrate the reduction in hydrogen atom concentration and increase in hydrogen molecule concentration with addition of CF_3I.

Figure 4: Calculated mole fractions of iodine containing species in the 0.006 mole fraction CF_3I doped stoichiometric hydrogen oxygen flame at P=30.0 torr.

Figure 5: Calculated temperature and reaction rates of progress for the three fastest iodine containing reactions in a laminar, burner-stabilized, stoichiometric, 30.0 torr hydrogen/oxygen flame with 0.006 mole fraction CF_3I.

Figure 6: Calculated temperature and reaction rates of progress for the remaining significant iodine containing reactions in a laminar, burner-stabilized, stoichiometric, 30.0 torr hydrogen/oxygen flame with 0.006 mole fraction CF_3I.

Figure 7: Schematic summary of the iodine reaction pathways in the CF_3I doped hydrogen/oxygen flame. The darker arrows denote the paths with faster peak reaction rates.

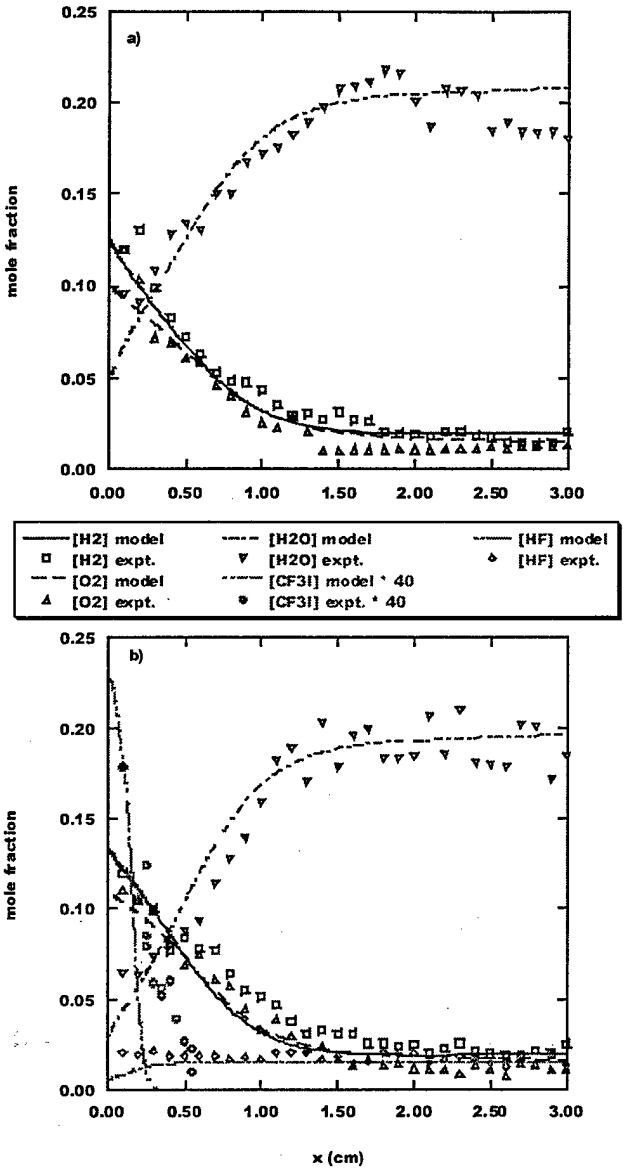
a)
b)
mole fraction
x (cm)
0.25
0.20
0.15
0.10
0.05
0.00
0.00
0.50
1.00
1.50
2.00
2.50
3.00
[H2] model
[H2] expt.
[O2] model
[O2] expt.
[H2O] model
[H2O] expt.
[CF3I] model * 40
[CF3I] expt. * 40
[HF] model
[HF] expt.

Figure 1

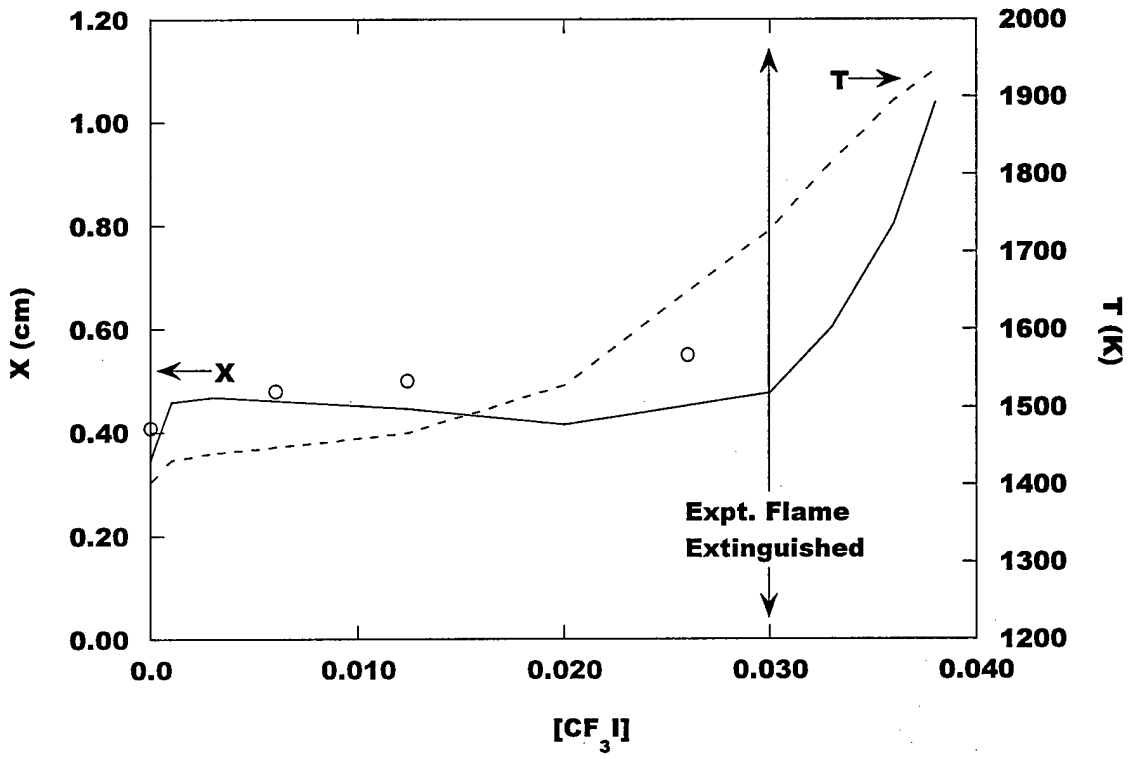
1.20
1.00
0.80
0.60
0.40
0.20
0.00
X (cm)
2000
1900
1800
1700
1600
1500
1400
1300
1200
T (K)
T
X
Expt. Flame
Extinguished
0.0
0.010
0.020
0.030
0.040
[CF3I]

Figure 2

Figure 3

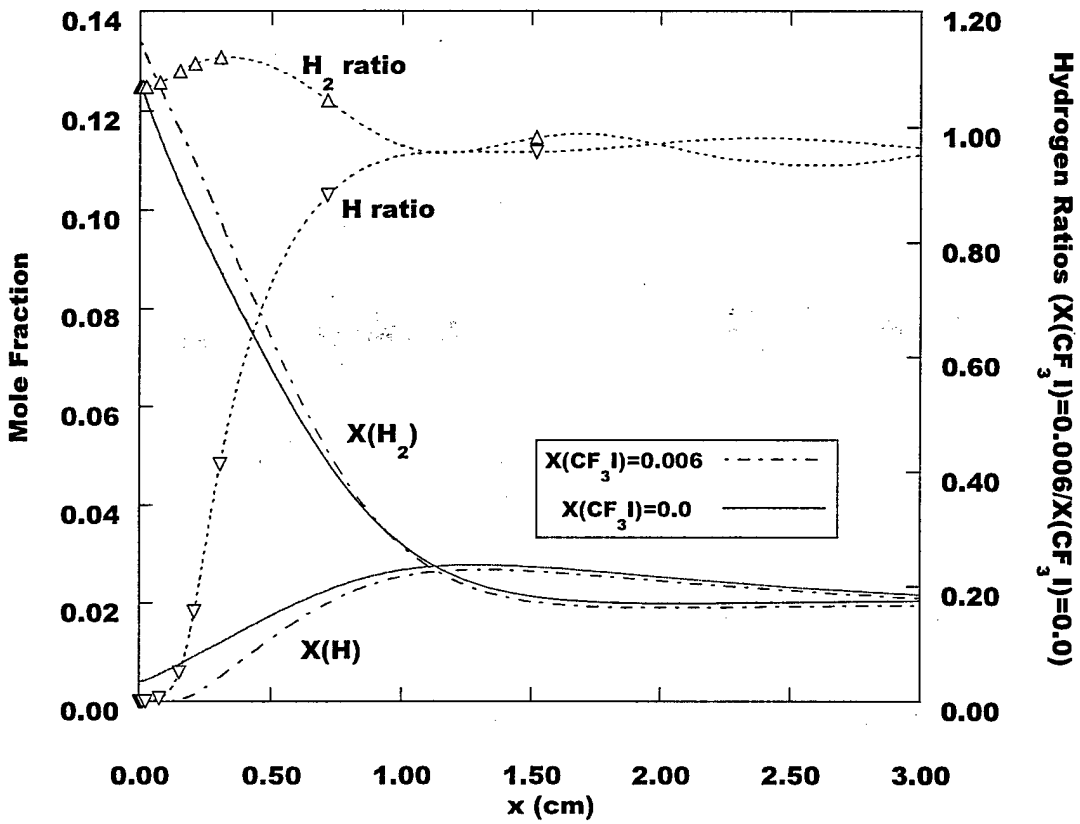
0.14
0.12
0.10
0.08
0.06
0.04
0.02
0.00
Mole Fraction
1.20
1.00
0.80
0.60
0.40
0.20
0.00
Hydrogen Ratios (X(CF3I)=0.006/X(CF3I)=0.0)
H2 ratio
H ratio
X(H2)
X(H)
X(CF3I)=0.006
X(CF3I)=0.0
0.00
0.50
1.00
1.50
2.00
2.50
3.00
x (cm)

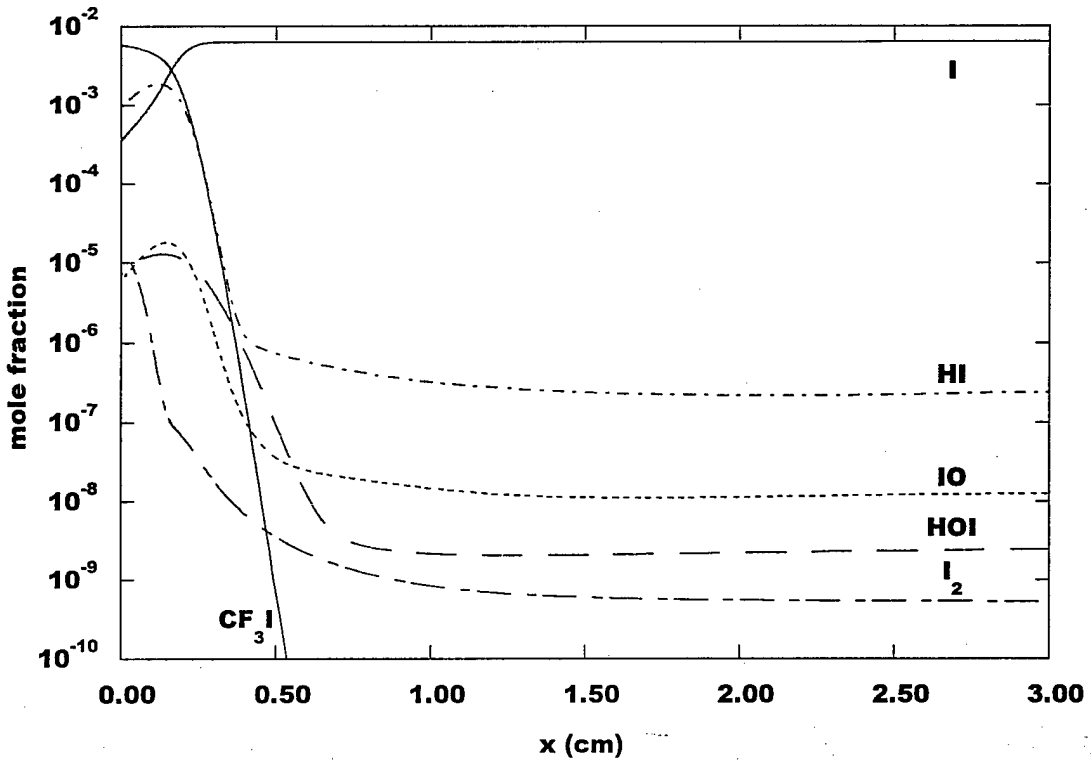
mole fraction
10-2
10-3
10-4
10-5
10-6
10-7
10-8
10-9
10-10
I
HI
IO
HOI
I2
CF3I
0.00
0.50
1.00
1.50
2.00
2.50
3.00
x (cm)

Figure 4

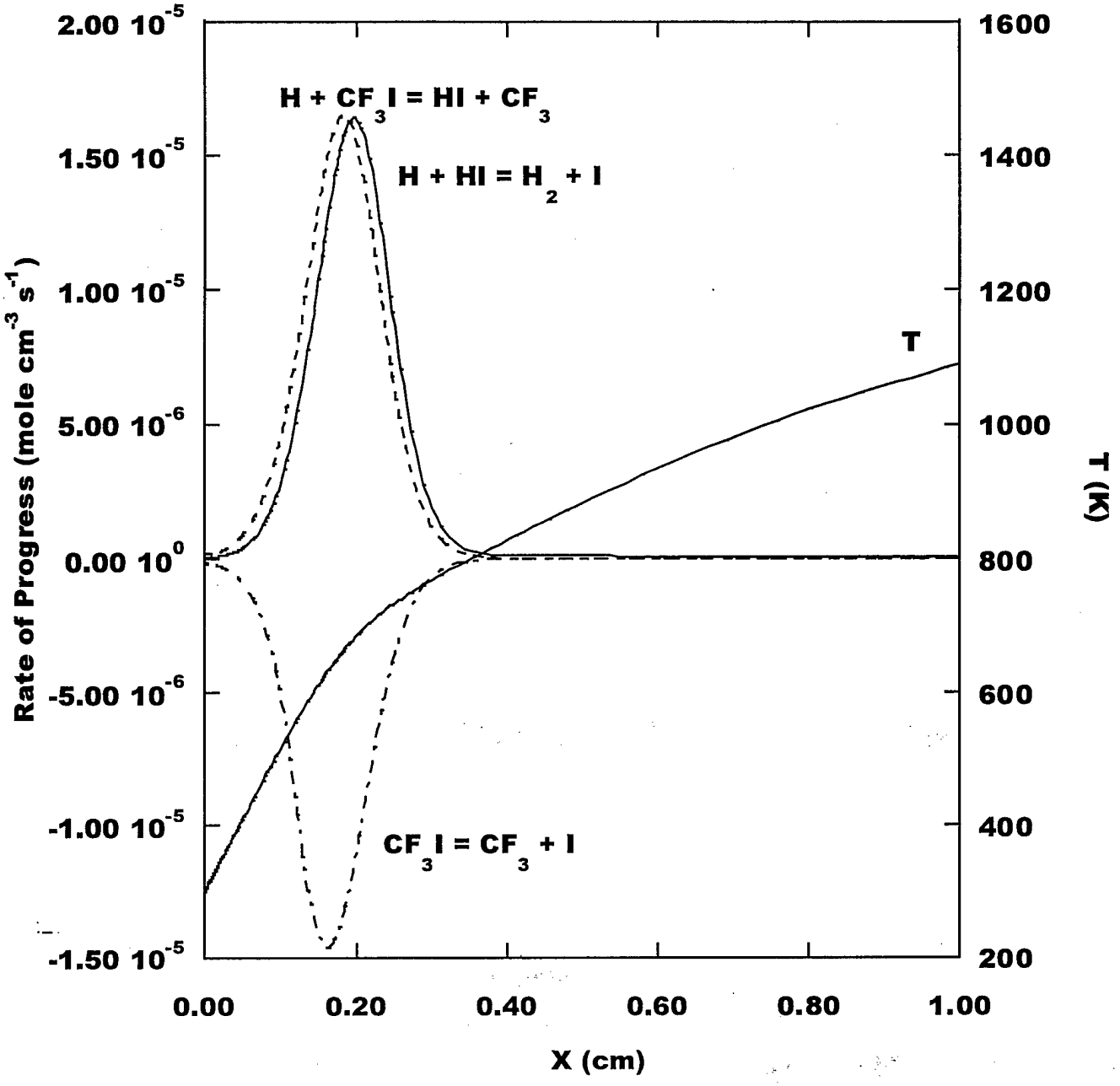
H + CF3I = HI + CF3
H + HI = H2 + I
CF3I = CF3 + I
T
Rate of Progress (mole cm-3 s-1)
T (K)
X (cm)
2.00 10-5
1.50 10-5
1.00 10-5
5.00 10-6
0.00 100
-5.00 10-6
-1.00 10-5
-1.50 10-5
1600
1400
1200
1000
800
600
400
200
0.00
0.20
0.40
0.60
0.80
1.00

Figure 5

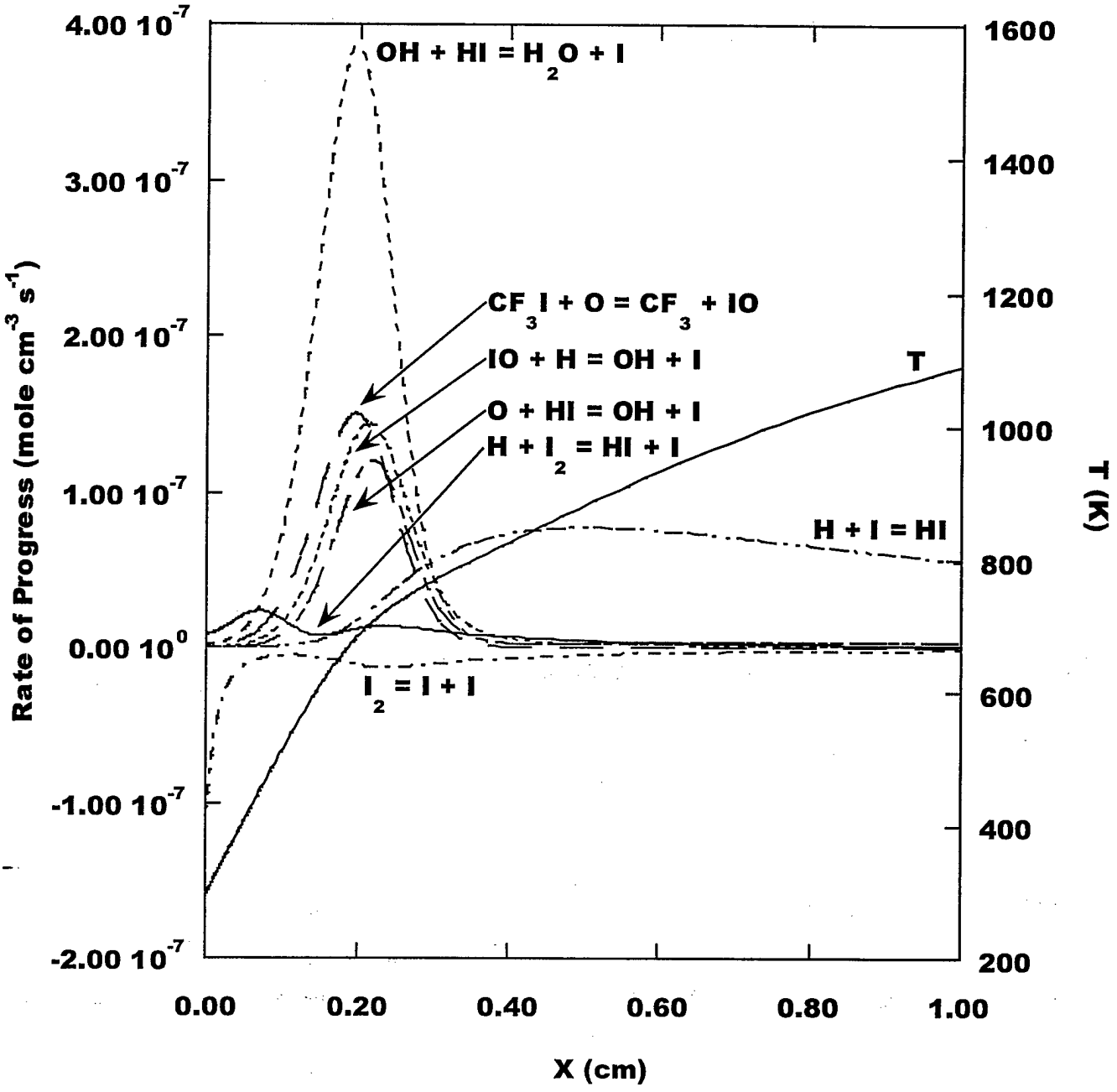
4.00 10-7
3.00 10-7
2.00 10-7
1.00 10-7
0.00 100
-1.00 10-7
-2.00 10-7
Rate of Progress (mole cm-3 s-1)
OH + HI = H2O + I
CF3I + O = CF3 + IO
IO + H = OH + I
O + HI = OH + I
H + I2 = HI + I
H + I = HI
I2 = I + I
T
1600
1400
1200
1000
800
600
400
200
T (K)
0.00
0.20
0.40
0.60
0.80
1.00
X (cm)

Figure 6

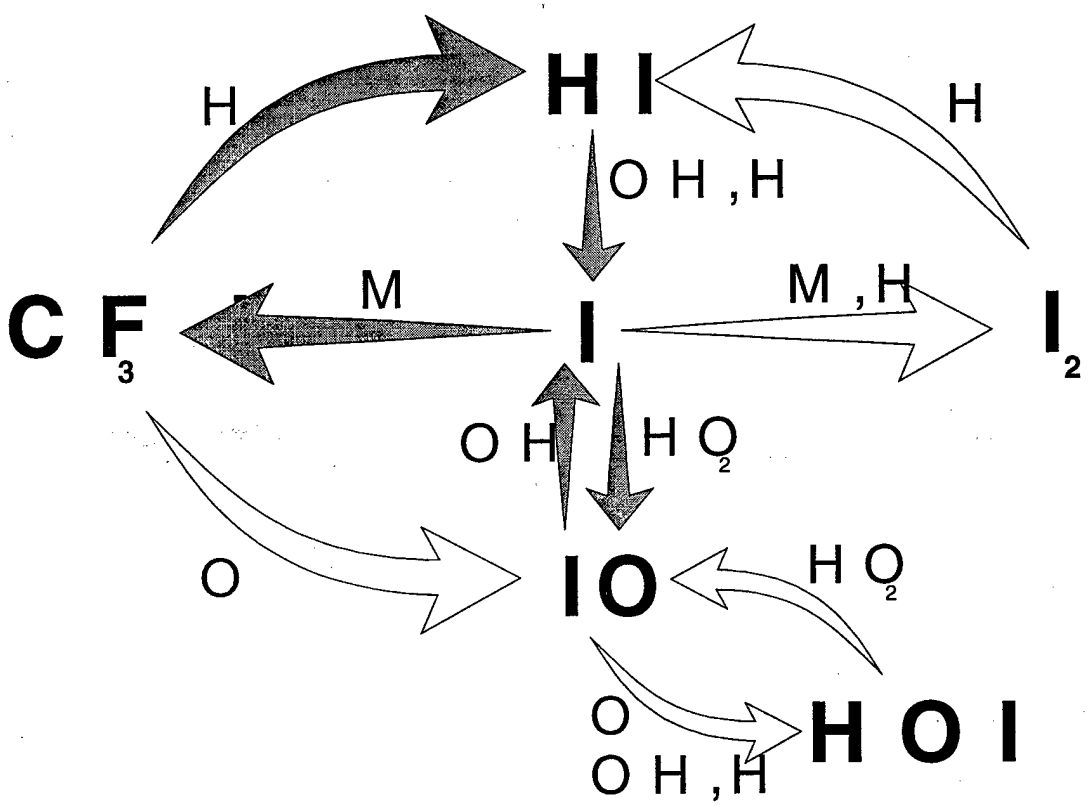

Figure 7

Report Number (14) SAND--98-8451C
CONF-980804--

Publ. Date (11) 199803
Sponsor Code (18) DOE/EE, XF,
UC Category (19) UC-1409, DOE/ER